ELSEVIER

Surface and Coatings Technology 155 (2002) 21–32

SURFACE & COATINGS TECHNOLOGY

www.elsevier.com/locate/surfcoat

Young's modulus and fracture toughness determination of high velocity oxy-fuel-sprayed bioceramic coatings

H. Li[a], K.A. Khor[a,*], P. Cheang[b]

[a]*School of Mechanical & Production Engineering, Nanyang Technological University, 50 Nanyang Avenue, Singapore 639798, Singapore*
[b]*School of Materials Engineering, Nanyang Technological University, 50 Nanyang Avenue, Singapore 639798, Singapore*

Received 23 May 2001; accepted in revised form 14 January 2002

Abstract

Indentation tests along with three- and four-point bend tests were utilized for the determination of Young's modulus (E) of high velocity oxy-fuel (HVOF) sprayed hydroxyapatite (HA) and HA/titania (TiO_2) coatings. In addition, fracture toughness (K_{Ic}) and strain energy release rates (G) with reference to the coating/substrate interface were investigated using the indentation technique and four-point bend test, respectively. Results showed that the E values of the bioceramic coatings were significantly dependent upon microstructure and phase composition. The incorporation of titania (10 and 20 vol.%) as reinforcements, which had higher stiffness than HA, was found to effectively improve the overall E values and fracture toughness of the composite coatings. It was revealed that the splats' interface played a substantial role in determining the fracture toughness on the assumption that cracks propagated predominantly along the interface. The present study claimed that the indentation test was essentially a local-phase-dependent method and was markedly influenced by surface roughness of the samples. The three- and four-point bend tests were found to be relatively more reliable for the evaluation of overall bulk property of the coating. And typical E values obtained from the three-point bend test were notably close to those obtained from the four-point bend test. It was found that the four-point bend test was not suitable for the determination of fracture energy at the coating/substrate interface due to the poor cohesion of the bioceramic coatings.

Keywords: Bending test; Hydroxyapatite; Indentation test; Young's modulus; Fracture toughness; Bioceramic coating; High velocity oxy-fuel

1. Introduction

Hydroxyapatite (HA) and its composite coatings on titanium alloy substrates have the potential for chemical bonding with bony tissues, and, have a high interface shear strength with bone [1]. In addition to the prerequisite of bioactivity, the complex service of the prosthesis requires that the coating be capable of withstanding applied physiological loads without any failure especially over long-term usage. Among the mechanical properties, elastic modulus (E) and fracture toughness (K) play a significant role in determining the duration and functional life of the thermal sprayed deposits as implants. Moreover, bioceramics coatings have the intrinsic problem of an additional interface being introduced into the system, which could act as a failure site as revealed through previous in-vivo and in-vitro studies [2–4]. The coating/substrate interface is an important determining factor in the reliability of the implants [5–7]. Therefore, it is believed that, besides biomechanical factors and tissue reactions at the implant–tissue interface, the success of implantation is strongly dependent on a satisfactory coating/substrate interface. So far the coating/substrate interface is generally evaluated by measuring the fracture energy at the interface [8–10].

Thermal sprayed coatings demonstrate marked incongruity in E values from corresponding bulk material due to their identified inhomogeneous layered structure, and the Young's modulus of coatings is essentially dependent on coating microstructure [11–13]. Most available techniques employed for evaluation of mechanical properties of thermal spray coatings have been discussed by Lin and Berndt [14]. The available method for the measurement of Young's modulus in coatings is limited due to its low thickness ($\sim$80–200 μm). A frequently adopted

*Corresponding author. Tel.: +65-790-5526; fax: +65-792-4062.
E-mail address: mkakhor@ntu.edu.sg (K.A. Khor).

0257-8972/02/$ - see front matter
PII: S0257-8972(02)00026-9

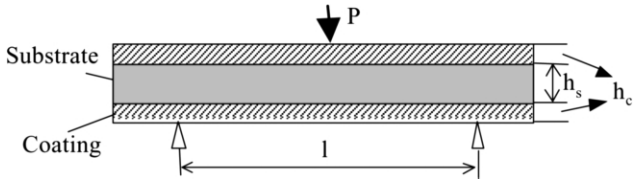

Fig. 1. Schematic depiction of the three-point bend test for Young's modulus determination of the coatings.

method for determining the Young's modulus of surface coatings and thin films is the indentation technique [12] owing to its simplicity in sample preparation. Other methods, such as bending tests have also been attempted [15–18]. Compared with the single-side coated specimen [16], the double-side coated specimen, which Fawcett first proposed for thick films, seems to have better accuracy [18]. Furthermore, non-destructive testing (NDT) approach, such as scanning acoustic microscopy [19,20], has also been used on thermal sprayed coatings and thin films in determination of E values.

Fracture toughness plays a decisive role in implant functionality by determining the level to which the material can be stressed in the presence of cracks, or, equivalently, the magnitude of cracking which can be tolerated at a specific stress level. Fracture toughness determination in coatings and thin films is usually based on an indentation technique [21–23]. An alternative way to evaluate the fracture property of a coating/substrate interface is to measure the critical strain energy release rate (G_{ss}) [9,24]. This method is extremely useful in the recognition that analysis of failed implants demonstrated primary failure on the HA/metal interface rather than on the bone/HA interface [25]. However, the dependability of the various methods involved in the determination of Young's modulus and fracture toughness of coatings is still being debated. A systematic investigation is therefore beneficial to elucidate the reliability of these methods for thermally sprayed coatings.

The present study aims to experimentally determine the Young's modulus and fracture toughness of high velocity oxy-fuel (HVOF)-sprayed HA and HA/TiO_2 coatings using the methods mentioned above. The different techniques were subjected to a comparative analysis. Furthermore, the influence of coating microstructure on the investigated variables was considered.

1.1. Theoretical background

1.1.1. Three-point bending for E determination

This method is based on the neutral axis maintaining its original position achieved through a double-side sprayed specimen during the bending test (Fig. 1). The symmetry during bending can be ascertained while the coatings on both sides are of similar thickness. The following formula is used to calculate the Young's modulus, E [18]:

$$2E_cI_c+E_sI_s=\frac{Pl^3}{48d} \tag{1}$$

where I is inertia moment, P and d is the load and corresponding displacement in the elastic scope during the bending test. l is the span. The subscript c and s represent the coating and the substrate, respectively.

$$I_s=\int_{-h_s/2}^{h_s/2} y^2bdy, \quad I_c=\int_{h_s/2}^{(h_s/2)+h_c} y^2bdy \tag{2}$$

The benefit of this method is that the E value obtained represents the overall property of bulk coating.

1.1.2. The four-point bend for E determination

The four-point bend test is conducted on a one-sided coating sample with a strain gauge attached on the substrate and the formula for E value determination was derived by Chiu [26]. Fig. 2 shows the depiction of the four-point bend test and the strain gauge set-up. Some assumptions were made in deriving the equation for Young's modulus of ceramic coating using this method:

- the coating–substrate bonding is perfect (plane strain);
- the samples are linearly elastic;
- there is no stress relaxation due to plastic deformation and microcracking during sample preparation;
- the Young's modulus is only dependent on the magnitude of stress and independent of the sign of stress; and
- load and support points are frictionless and do not introduce local crushing or wedging stresses.

During bending of the sample, by using the tangent rule, it can be deduced that: [26]

$$l=l_s-\left(\frac{K}{1+K}\right)(l_s+l_c) \tag{3}$$

where l_c and l_s are the thickness of coating and substrate, respectively, l is the distance from the neutral axis to the coating-substrate interface, $K=-\frac{\varepsilon_s}{\varepsilon_c}$ is defined as

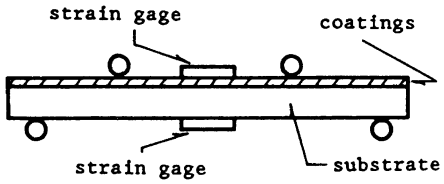

Fig. 2. Schematic depiction of the four-point bend test and strain gauge set-up for the E determination.

relative strain. Using stress equilibrium,

$$\int_{-l}^{l_s-l} \sigma_s dA + \int_{-l-l_c}^{-l} \sigma_c dA = 0 \quad (4)$$

where A is the cross-sectional area. The normal surface stress is calculated by

$$\sigma_c = \frac{E_c y}{r}, \quad \sigma_s = \frac{E_s y}{r} \quad (5)$$

where r is the radius of curvature of the neutral axis, σ_c and σ_s are the surface (normal) stress on the coating and substrate, respectively.

Combining Eqs. (3)–(5), the following formula can be derived:

$$E_c = E_s R \frac{KR + 2K - R}{2R - K + 1} \quad (6)$$

where $R = \frac{l_s}{l_c}$ is defined as the relative thickness. The relative strain K was calculated using the equation:

$$K = \frac{\sum_1^n K_n}{n} = \frac{\sum_1^n \left(-\frac{\varepsilon_s(n)}{\varepsilon_c(n)} \right)}{n} \quad (7)$$

where n is the number of measurements when the load is above 100 N, to eliminate excessive measurement error at lower load values. The average value of individual relative strain was taken to give a representative value for K across the entire range.

1.1.3. Indentation test for E determination

The principle of this method is based on the elastic response of materials when a loading indenter is applied to the specimen (Fig. 3). In the figure, P is applied load, h_c and h_f represent contact depth, final depth, respectively. The apparent elastic modulus of the sample, E^*, is calculated from the load-displacement curve using standard Hertzian contact theory: [27]

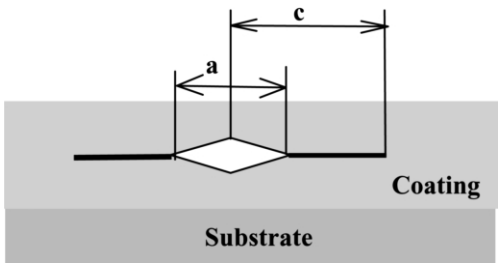

Fig. 4. Schematic depiction of the micro-indentation test for E determination.

$$E^* = \left(\frac{9}{16} \right)^{\frac{1}{2}} P h^{-\frac{3}{2}} R^{-\frac{1}{2}} \quad (8)$$

where h is the depth of elastic penetration of the indenter, P is the load, and R is the indenter radius. The true modulus of the sample, E can be calculated from the apparent modulus by taking into account the elastic properties of the indenter:

$$E = \frac{1 - \upsilon^2}{(1/E^*) - \left[(1 - \upsilon_i^2)/E_i \right]} \quad (9)$$

where υ is Poisson's ratio, and the subscript i refers to the indenter.

1.1.4. Indentation test for K_{Ic} determination

The principle of this method is based on the ability of coatings to inhibit crack propagation. The test for the determination of fracture toughness (K_{Ic}) is illustrated schematically in Fig. 4. A Vickers load is applied on a polished cross-section of the coating and the crack-lengths induced by the indentation are subsequently measured. The following formula is utilized for the determination of the fracture toughness [23]:

$$K_{Ic} = 0.016 (E/H)^{1/2} (P/C^{3/2}) \quad (10)$$

where E is the Young's modulus of the coating, H is

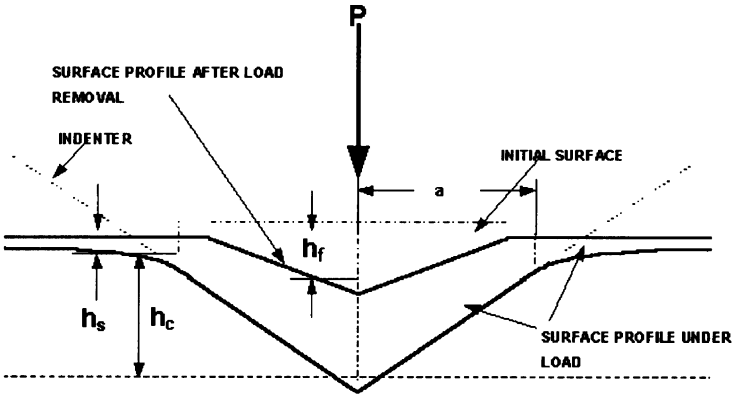

Fig. 3. Schematic diagram of Vickers' indentation test for the determination of fracture toughness.

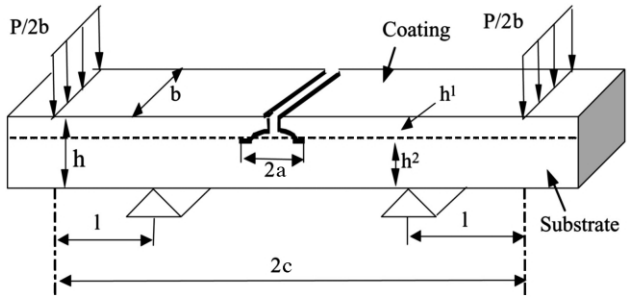

Fig. 5. Schematic illustration of the bimaterial specimen for four-point bending test.

the hardness of the coating, C is the crack length caused by indentation, and P is the indenter load.

1.1.5. Four-point bend test for G determination

The specimen loaded by four-point bending for the determination of the strain energy release-rate (G) with reference to the coating/substrate interface is depicted in Fig. 5. G can be obtained from the strain energy per unit cross-section, U, according to beam theory under plane strain conditions:

$$G=\frac{\partial U}{\partial a} \tag{11}$$

where a is the propagated crack length. The critical strain energy release rate (G_{ss}) during crack propagation can be expressed in the non-dimensional form: [28,29]

$$G_{ss}=\frac{M^2(1-\nu_2^2)}{2E_2}\left(\frac{1}{I_2}-\frac{\lambda}{I_c}\right) \tag{12}$$

where E is the Young's modulus, I is the inertia moment, ν is Poisson's ratio, and

$$M=Pl/2b \tag{13}$$

$$\lambda=E_2(1-\nu_1^2)/E_1(1-\nu_2^2) \tag{14}$$

$$I_c=h_1^3/12+\lambda h_2^3/12 + \lambda h_1 h_2(h_1+h_2)^2/4(h_1+\lambda h_2) \tag{15}$$

$$I_2=h_2^3/12 \tag{16}$$

In order to determine G_{ss}, both the applied load and the displacement of the loading points are continuously monitored and recorded. The specimen was loaded until both cracks had propagated out to the supporting points. Stable crack advance should ideally occur at a constant load, whereas a crack burst causes a sharp drop in load between two values having a mean of P_c [10]. A combination of several modes, particularly Mode I and Mode II often opens the cracks located along the interface of two materials.

2. Experimental procedures

Several types of HA and HA/TiO_2 coatings were prepared on Ti-6Al-4V substrate for the investigation. These are tabulated in Table 1. For the purpose of revealing the extensive influence of phase composition and post-spray heat treatment on Young's modulus values, as-sprayed, heat-treated and composite coatings were investigated. The HV2000 HVOF (Praxair, USA) system with a nozzle diameter of 19 mm was used for the coating deposition. Hydrogen was utilized as the primary fuel gas. For all the coating sample preparations, the powder carrier gas was argon with a flow rate of 19 l/min and the powder feed rate was 6 g/min.

Samples used for the indentation test to determine E values from the coating surface were ground and polished with 1-μm diamond paste before each test. Surface roughness was measured in terms of R_a using a surface roughness analyzer (Mitutoyo SURF TEST SV-600). R_a is the arithmetic mean of the absolute departures of the roughness profile from the mean line, which is normally a line which bisects the profile such that the areas above it and below it are equal. A relatively generous scanning length of 12 mm was adopted for a mean R_a value. The indentation test for the determination of E values was performed using Vickers micro-indentation equipment (CSEM® MHT, Switzerland). The maximum load was 1 N with a loading rate of 1 N/min and the duration was 10 s. The unloading rate was also 1 N/min. During the indentation test for E determination, every two points had a distance of 500 μm, which was sufficiently long to avoid the stress–strain influence caused by the previous loading of the preceding indentations. Since the phase in the present HA coatings is essentially crystalline HA, the Poisson's ratio (ν) of pure HA coatings was assumed to be 0.28. [30] The Poisson's ratio of titania is 0.278 [31], and because the content of titania in the composite coating was relatively small ($\leq$20 vol.%), it was also assumed that the overall Poisson's ratio of the HA/titania composite coating was 0.28 for related calculations. The elastic properties of the diamond indenter used in the calculations were E_i= 1141 GPa and υ_i=0.07 according to the CSEM Microhardness Tester Manual. A total of 15 points were averaged for every sample.

For the determination of Young's modulus utilizing the bending tests, an E value of 113 GPa for Ti-6Al-4V was employed and the coating thickness was ~180 μm. The dimension of the substrate for the three-point bending test was 120 mm×20 mm×2 mm in length, width and thickness, respectively. Three samples were prepared for the bend test for each type of coating. For the three-point bend test, three bending curves were obtained by choosing different positions for every sample. The tests were performed using a universal-testing machine (Instron model 5569 with a 500 N load). For

Table 1
Coating samples used for the investigation of Young's modulus and fracture toughness

Coating designation	Starting components	Spray parameters	Phase composition	Crystallinity (%)	Sample condition
H-1	HA (50 ± 5 μm)	Flow of O_2: 236 l/min Flow of H_2: 566 l/min SD: 210 mm	Mostly HA	98	As-sprayed
H-2	HA (50 ± 5 μm)	Flow of O_2: 283 l/min Flow of H_2: 566 l/min SD: 250 mm	Mostly HA	90	As-sprayed
H-3	HA (50 ± 5 μm)	Flow of O_2: 283 l/min Flow of H_2: 519 l/min SD: 250 mm	Mostly HA	98	As-sprayed
H-4	HA (30 ± 5 μm)	Flow of O_2: 283 l/min Flow of H_2: 566 l/min SD: 250 mm	HA + TCP	41	As-sprayed
H-4h	HA (30 ± 5 μm)	Flow of O_2: 283 l/min Flow of H_2: 566 l/min SD: 250 mm	HA + TCP	41	500 °C (30 min)
H-4c	HA (30 ± 5 μm)	Flow of O_2: 283 l/min Flow of H_2: 566 l/min SD: 250 mm	HA	100	750 °C (30 min)
H-5	HA (40 ± 5 μm)	Flow of O_2: 283 l/min Flow of H_2: 566 l/min SD: 250 mm	Mostly HA + TCP	85	As-sprayed
H-5c	HA (40 ± 5 μm)	Flow of O_2: 283 l/min Flow of H_2: 566 l/min SD: 250 mm	Mostly HA + TCP	100	750 °C (30 min)
C-6	90 vol.% HA-10 vol.% TiO_2	Flow of O_2: 283 l/min Flow of H_2: 566 l/min SD: 250 mm	HA, TiO_2, $CaTiO_3$, TCP	100	As-sprayed
C-6h	90 vol.% HA-10 vol.% TiO_2	Flow of O_2: 283 l/min Flow of H_2: 566 l/min SD: 250 mm	HA, TiO_2, $CaTiO_3$, TCP	100	450 °C (30 min)
C-7	90 vol.% HA-10 vol.% TiO_2	Flow of O_2: 283 l/min Flow of H_2: 566 l/min SD: 250 mm	HA, TiO_2, $CaTiO_3$, TCP	100	As-sprayed
C-7h	90 vol.% HA-10 vol.% TiO_2	Flow of O_2: 283 l/min Flow of H_2: 566 l/min SD: 250 mm	HA, TiO_2, $CaTiO_3$, TCP	100	450 °C (30 min)
C-8	80 vol.% HA-20 vol.% TiO_2	Flow of O_2: 283 l/min Flow of H_2: 566 l/min SD: 250 mm	HA, TiO_2, $CaTiO_3$, TCP	100	As-sprayed
C-8h	80 vol.% HA-20 vol.% TiO_2	Flow of O_2: 283 l/min Flow of H_2: 566 l/min SD: 250 mm	HA, TiO_2, $CaTiO_3$, TCP	100	450 °C (30 min)

SD, spray distance; TCP, $Ca_3(PO_4)_2$; the amount of different phases in the coatings can be found in the literature [34,38], for the composite coatings, for C-6 and C-6h, HA has a particle size of 50 ± 5μm, for C-7, C-7h, C-8 and C-8h, HA has a particle size of 40 ± 5μm, and the titania particle has a mean diameter of 1 μm.

the three-point bend test, the bending rate was 0.2 mm/min and a set of load-displacement data was chosen for the calculation of E within the elastic deformation regime. For the four-point bend test, the span was 22.5 mm between the top load points and 45 mm between the bottom support points. The plate sample was of a dimension of 60 mm in length and 6 mm in width. A total of 20 sets of data were recorded for each sample ($n=20$) through manually controlling the loading step by step. For the purpose of accurate determination of E value, the tested coatings/substrates were sectioned using a diamond blade after the bending test, the thickness of coating and substrate was accurately measured under an optical microscope with high magnification ($200\times$).

In the determination of fracture toughness using the indentation technique, the indenter load, P, was 0.5 N with a load application time of 15 s in the present study. A total of 15 points were collected for each type of coating. The experiment was conducted on the HMV-2000 Shimadzu microhardness tester.

For the four-point bending test, it was pointed out that the pre-crack length, a, has a significant effect on the strain energy release rate [32]. And if the specimen

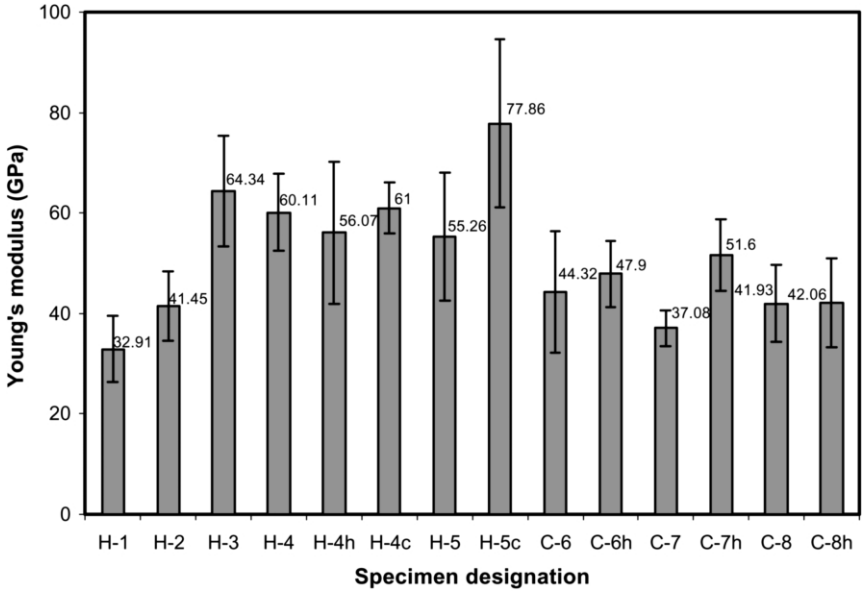

Fig. 6. Young's moduli of investigated HA and HA/titania coatings using indentation test.

dimension is in the range, $0.05 \leq h_1/H \leq 0.5$, a steady state behavior is essentially obtained for interface cracks in the extensive crack length range $0.2h_1 \leq a \leq 0.9(c-1)$ [33]. In this study, the specimen shown in Fig. 5 has the following parameters: $2a = 10$ mm, $h_1 = 0.320$ mm, $h_2 = 1.95$ mm, $b = 2$ mm, $2c = 80$ mm, $l = 20$ mm. The pre-crack was prepared by putting a masking strip with a width of 5 mm on the substrate to prevent the local substrate from sandblasting. After the coating deposition, a wire saw was used to produce a notch in the coating along the central line. Subsequently, a three-point bending was performed on the Instron universal-testing machine with a support span of 10 mm to prepare the pre-crack with a length of 10 mm. The bending speed was 1 mm/min for both the three- and four-point bending tests.

3. Results and discussion

3.1. Young's moduli of investigated coatings

The E values obtained in the indentation tests are illustrated in Fig. 6. It is noted that the error for each of the coatings is considerably large, which may suggest the influence of surface condition on the precision of the measurement. Further investigation shows that coating surface roughness indeed plays an important role on the E, as depicted in Fig. 7. The corresponding improve-

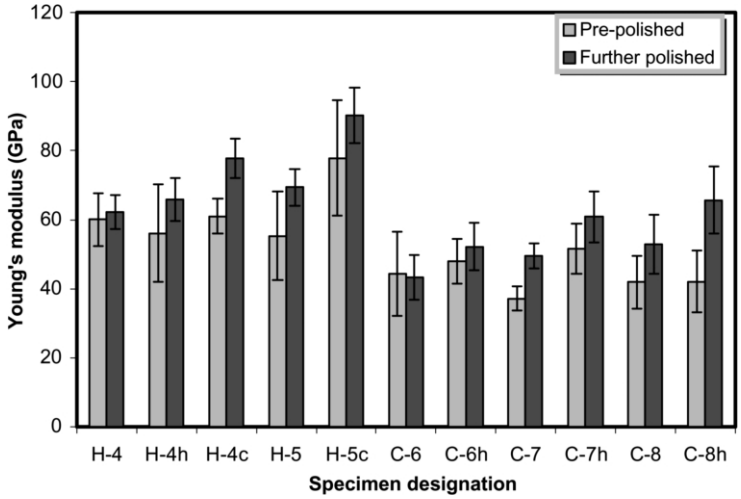

Fig. 7. Influence of surface roughness on E obtained through indentation test.

Table 2
Comparison of elastic moduli of investigated coatings corresponding to different surface roughness

Coating designation	R_a (μm)	E (GPa)	R_a' (μm)	E' (GPa)
H-4	0.306	60.11±7.65	0.299	62.23±4.83
H-4h	0.732	56.07±14.17	0.353	65.82±6.32
H-4c	0.315	61.00±5.03	0.222	77.67±5.69
H-5	0.318	55.26±12.83	0.221	69.33±5.24
H-5c	0.920	77.86±16.74	0.807	90.21±8.02
C-6	1.075	44.32±12.06	0.940	43.28±6.55
C-6h	1.086	47.90±6.56	0.646	52.19±6.85
C-7	0.655	37.08±3.49	0.345	49.47±3.56
C-7h	0.966	51.60±7.16	0.697	60.86±7.35
C-8	0.971	41.93±7.66	0.482	52.92±8.67
C-8h	0.937	42.06±8.87	0.373	65.69±9.83

ment of surface roughness brought by finely polishing the coating surface is tabulated in the Table 2. As demonstrated in Fig. 7, the additional polishing of coating's surface, which causes a further decrease of R_a, results in an increase in E values and the standard deviation is found to decrease subsequently. Therefore, it can be concluded that no reliable comparison among the different coatings can be made, as identical surface roughness values (R_a) cannot be pragmatically achieved for all the coatings. Fig. 8 shows the morphology of the crater induced by the indentation of two types of HA coatings, H-4 and H-5, which are of different R_a values. It is clearly found that once the surface is reasonably smooth, as shown in Fig. 8a, no microcracks around the crater can be seen. This indicates that the E value obtained is quite acceptable. However, as the coating structure is significantly dependent upon the starting HA powder size [34], a low R_a value for H-5 coating cannot be easily achieved. And it is possible that titania particles in the composite coatings can be pulled out during metallographic polishing, which results in an irregular surface. Therefore, the indentation method can only be used for the coatings with a low porosity level and with an exceedingly smooth and regular surface through meticulous metallographic polishing. Furthermore, the large deviation demonstrated by all the coatings suggests that this indentation process is a local phase-dependent method. This method is not capable of producing comparative values.

The E values obtained through three-point bend tests for the selected coatings are illustrated in Fig. 9, in which the E values of H-2, H-4, H-5 coatings via four-point bending are also demonstrated. It should be noted that the test was conducted on the as-sprayed coatings without any surface treatment. It was found that a large starting HA powder size results in a high E value. Post-heat-treatment is beneficial for the improvement of E values. And the addition of titania effectively increases the E values of HA-composite coatings. The results

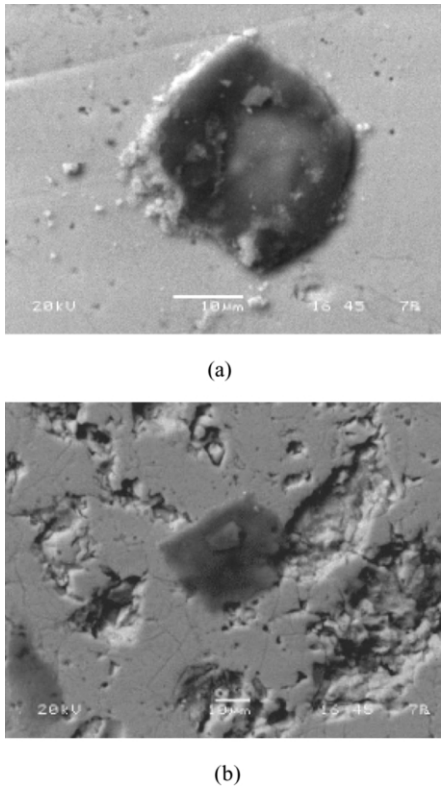

Fig. 8. Typical morphology of the crater induced by indentation for the determination of Young's modulus showing the influence of surface roughness: (a) H-4 coating with lower porosity; and (b) H-5 coating with higher porosity.

obtained from the three-point bend test correspond well to those obtained from the four-point bend tests. Compared with the E values shown in Figs. 6 and 7, the improvement induced by the incorporation of titania was not conclusive. The reason may be due to the dependency of E values obtained using indentation tests on local phase composition.

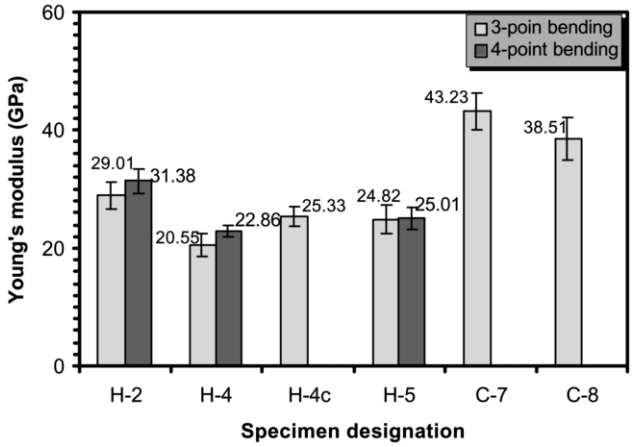

Fig. 9. Elastic moduli of investigated coatings through three- and four-point bend tests.

The improvement of E due to the annealing heat treatment is believed to be partially caused by the releasing of residual stresses formed during coating deposition, which was believed to be the major factor in determining the Young's modulus of thermal-sprayed HA materials [35]. However, the influence of residual stresses on E values during measurement is still debatable. Furthermore, the crystallization that accompanied the heat treatment contributes to the increased E, on the basis that crystallization of amorphous calcium phosphate to HA results in a crystallographic change [36]. Moreover, the improvement of structure could significantly contribute to the increased E [11,13].

Fig. 9 shows that the Young's modulus of the composite coating, which composed of 10 vol.% TiO_2 (C-7) nearly satisfies the classical linear rule-of-mixture (ROM) relationship when compared with the unreinforced HA coating H-5, [37]. Which essentially describes the response of particulate reinforced composite materials without the consideration of the contribution from defects and chemical products in the coating:

$$E_c = E_p V_p + E_m V_m \quad (17)$$

where E_c is the Young's modulus of the coating, V is the volume fraction, and the subscripts p and m represent secondary particles and matrix, respectively. In a previous report, it has been clarified that mutual reaction between HA and titania occurs during coating formation and the resultant phase, $CaTiO_3$, appears [38]. It is believed that while the TiO_2 content in HA coating is small, the influence of an additional interface and a third phase, namely $CaTiO_3$, is minimal. The improvement of the Young's modulus is attributed principally to the existence of TiO_2. However, the decrease of the Young's modulus in the composite coating with 20 vol.% TiO_2 indicates the considerable enhanced influence of the multi-phases in the coatings that resulted from chemical decomposition and mutual reactions.

It is noted that the E values obtained from the three- and four-point bend tests are markedly lower than those obtained from the indentation process. This can be explained by the intrinsic difference in principles that the bending test is based on the entire coating whereas the indentation test is primarily a local-phase-dependent method.

3.2. Fracture toughness and strain energy release rate

As discussed in Section 1.1.4, the fracture toughness calculated from Eq. (10) using the E values obtained from three-point bend test is based on the argument that the bending test yields an E value that reflects the coating's overall property. Fig. 10 shows the fracture toughness (K_{Ic}) of selected coatings. It reveals that the coating microstructure plays a marked role in determining the fracture property. However, it is found that HA

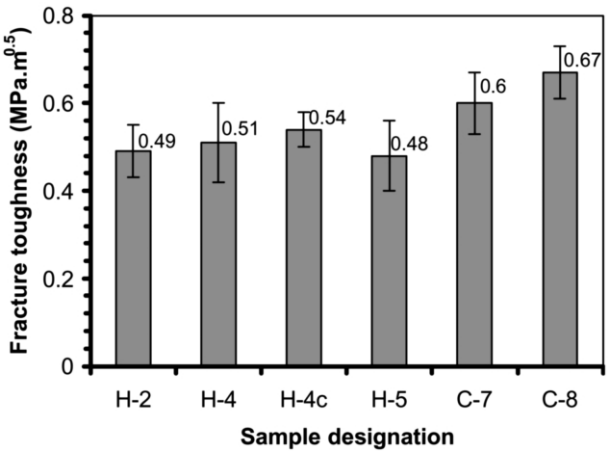

Fig. 10. Fracture toughness (K_{Ic}) of investigated coatings through the indentation test.

coatings deposited with small starting HA powder results in higher fracture toughness in the coating. And it shows that the fracture toughness, K_{Ic}, increases with an increasing amount of TiO_2 in HA coatings, from 0.48 ($\pm$0.08) MPa $m^{0.5}$ to 0.60 ($\pm$0.07) MPa $m^{0.5}$ and 0.67 ($\pm$0.06) MPa $m^{0.5}$, for 0%, 10 vol.% and 20 vol.% titania reinforcement, respectively.

The relatively high fracture toughness exhibited by the composite coatings compared with unreinforced HA coatings indicates the improved bonding area of the splats' interface. It is deemed that the mutual chemical reaction between the two components results in a higher overall density. It has also been pointed out that coating microstructure controlled its toughness and as the porosity increased, toughness decreased [39]. A study on HA/zirconia composites also revealed remarkable influence of the porosity on overall fracture toughness [40]. The present results are consistent with other reports on plasma-sprayed porous HA coatings in that as plasma power increased, and with a corresponding decrease in porosity levels, the HA/substrate interfacial fracture toughness increased [41]. The phases that resulted from the mutual reaction or chemical decomposition is likely located along the splats' interface and thus reduce the defects along the splats' interface, consequently improving the ability to inhibit crack propagation induced by the indenter. In this view, a well-melted state achieved by small HA particles in the HVOF flame is beneficial for the splats' bonding, and subsequently responsible for the improvement of K_{Ic} illustrated in Fig. 10. It can be deduced that the inter-lamellae cohesion is the most important factor, which significantly influences the fracture toughness. As the fracture along the lamella's interface can be used for the evaluation of the cohesive property among the splats to a certain extent, it can thus be postulated that the fracture toughness is arguably capable of demonstrating cohesion among the lamellae.

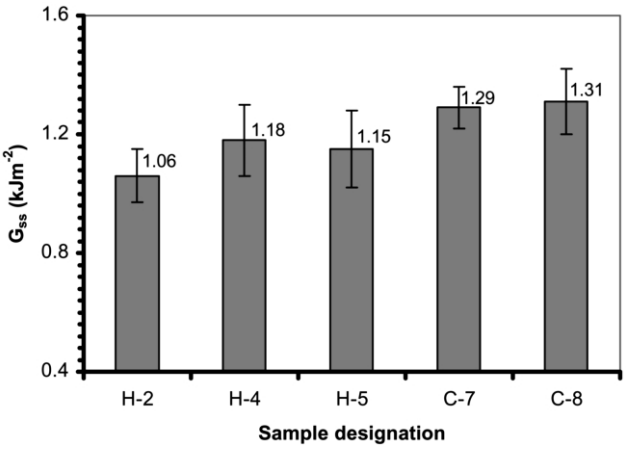

Fig. 11. Critical strain energy release rate (G_{ss}) of selected coatings obtained from the four-point bending test.

Considering the shape of the crack propagation trace, which is complex rather than linear, the determination of the crack length is indeed a perplexing problem, even though some researchers have measured the length for the calculation of the fracture toughness [42].

The G_{ss} values for selected coatings are shown in Fig. 11. Composite coatings show relatively higher G values than unreinforced HA coatings and HA coatings deposited using small HA powder results in a higher G value. It was pointed out that coating microstructure acted as an important factor in determining the fracture property or even failure location during fracture test of thermal sprayed coatings [39,43]. In order to reveal the effect of microstructure on G_{ss}, failure morphology is observed by means of a scanning electron microscope (SEM), which is shown in Fig. 12.

It is found that during the four-point bend test the crack propagates within the HA coating near the coating/substrate side. The wave-like worn surface together with the bending curve analysis indicates that kinking and trapping of the bending cracks occur during crack growth. Some HA coatings remained on the substrate with thicknesses that varied from several μm to approximately 20 μm depending on the location. According to the crack growth mechanism, which demonstrates that the cracks always propagate along the direction with minimum strain energy, the present crack propagation path supplies the minimum resistibility. According to Sih [44], once a crack is initiated, the fracture path follows the trajectory of points of minimum strain energy density remarkably closely. Considering the complex residual stresses and the applied stresses from the bending moment, shear stresses apart from tensile stress at the crack front, the crack propagation into the coating side can be explained in combination with likely intrinsic flaws, such as micropores and microcracks within the coating. Once the crack deviates from the linear path, it can be observed that it intervenes into the coating for a very short distance, and then the crack path returns back to the proximity of the interface zone, which suggests a possible maximum tensile stress at the interface.

Typical fracture morphology shown in Fig. 12 reveals that there is no evidence of cracking parallel to the surface of lamellae. There are, however, several fresh fracture surfaces in the form of trans-lamellar cracks. The trace of the brittle fracture indicates that the existing microcracks in the coating are connected together as the propagation path of the crack. Furthermore, the size and distribution of pores may also play a major role in influencing both the fatigue crack initiation and propagation processes [45]. The effect of the micropores during the crack propagation is demonstrated in Fig. 13. Two points can be obtained from the image, one is that the existence of micropores can effectively inhibit the propagation of cracks, while the other point is that the pores supply the necessary growth path for the cracks. Thus, the crack propagates between two adjacent pores. The effect of micropores that existed along the crack propagation path on the fracture toughness has been discussed by Leguillon [46]. It was believed that the crack growth was made of successive sudden jumps at

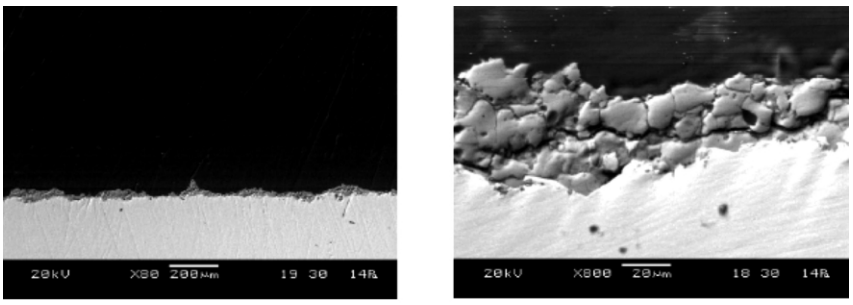

Fig. 12. Typical bending failure morphology of HA coating in the view of worn morphology (a) parallel to and (b) perpendicular to the crack growth direction showing that the crack totally propagates within the coating rather than the coating/substrate interface.

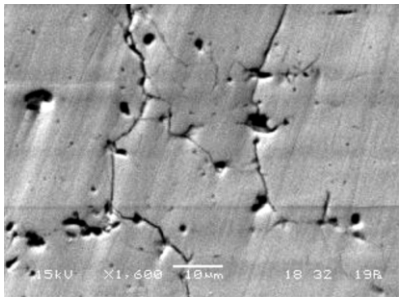

Fig. 13. Illustration of the connection of the micropores during the crack growth indicating the effect of coating porosity on its fracture toughness.

each void along the crack path. The relationship between the void size and stress intensity factor was presented as: [46]

$$k_{\mathrm{Ic}}^{\mathrm{eff}} = k_{\mathrm{Ic}}\sqrt{m} \tag{18}$$

where $m = 1 - \lambda/\varepsilon$; λ/ε is the porosity along the crack propagation path. Thus, the existence of micropores at the crack propagation path is detrimental to the fracture toughness.

In consideration that different spray parameters yield inconsistent porosity levels, the strain energy release rate which is different depending upon the different types of HA coatings can be explained by the final microstructure. High oxygen and hydrogen flow rates are beneficial for the improvement in terms of final density, as well as the powder choice. The fully melted state of the powder in the HVOF flame is useful for achieving low porosity in the coatings. Combining with a previous report that demonstrates coating failures in HVOF sprayed HA coatings as located preferably at the unmelted/melted part of single HA particle [34], it can be surmised that the strain energy release rate of a C-6 coating is higher than that of a C-4 coating.

Based on the presumption that the bending fracture occurred mostly within the HA coating near the coating/substrate interface, it is deemed that the fracture energy of coating/substrate interface is higher than that of the HA coating. This can be explained by the large quantities of defects existing in the coating rather than at the interface. Even though several studies have utilized the four-point bend test for the measurement of coating/substrate interface fracture toughness [10,47], there is thus far a lack of failure morphology analysis which is necessary for the relevant application of this method. It should be pointed out that this method is imperfect for the determination of fracture toughness because the formula used for the calculation of strain energy release rate is based on the assumption that the interface crack advances symmetrically during bending. Furthermore, the present G values are exceedingly high and it is possible that the G values are presumably crack-initiation dominated. Moreover, the excessive plastic deformation of the substrates could also contribute to the measured G values. The thickness ratio of the coating to the substrate seems to require a high value. Nevertheless, new methods must be explored for the strain energy determination with reference to the coating/substrate interface of the present thermal-sprayed bioceramic coatings.

It has been pointed out that the porosity of coating has a pronounced effect on overall Young's modulus of the coating [11,41], that is, the E value will largely decrease as the coating porosity increases. A recent study summarized two microstructural features, namely, microcracks and pores, for accounting the changes in Young's modulus of the ceramic coatings through plasma spraying extremely coarse HA powders [41]. The present study confirms the previous findings. Moreover, Leigh et al. [12] claimed that the reductions in the E values of thermal sprayed deposits were not only related to the porosity, in fact the pore morphology also had a significant influence on the reduction in the E values. The bonding state among the splats also plays a significant role. The thermal-sprayed coatings showed highly anisotropic elastic behavior, i.e. a higher E value parallel to the coating surface [12]. It has been claimed that the Young's modulus of coatings depends thoroughly on the orientational scatter and average aspect ratios of the pores and the partial porosities [11]. Moreover, the moduli decrease monotonically as porosity increases [11]. Concerning the indentation test for the determination of Young's modulus, it is a surface morphology related method and primarily characterizes the surface's property. While for the thermally-sprayed coatings it is difficult to achieve a very smooth surface as attributed to the different coating components, different coatings can only be ascertained as identified surface roughness together with the influence of spray process. Therefore, the Young's modulus data lose their reliability on the basis that they cannot be compared wholly. Meanwhile, during coating formation, many procedures bring about the formation of residual stresses within the as-sprayed coating and the value is dependent upon the location within the coating. It has been confirmed that residual stress plays an important role in the coatings Young's modulus properties. From this viewpoint, it can be stated that indentation test can only be used for superficial determination of Young's modulus and large quantities of points should be collected for a statistically acceptable value.

The three- point and four-point bending tests for the E determination can be called a macro-evaluation process. Thus, they can be used to determine the properties of bulk coating with all the considerable variables, which can typically influence Young's modulus. For the fracture toughness determination using the indentation test, different indenter loads were tried in the present study.

It was concluded that the load for the indentation test must be sufficiently small in order to assure the approximately linear cracks, which are used for K determination. As the load increases, the cracks demonstrate complicated shapes, thus it is difficult to establish an effective crack length for subsequent calculation.

For the purpose of accurately determining the property of HA-coating/Ti-6Al-4V-substrate interface, new evaluation method is required. However, new acceptable technique used specifically for thermal-sprayed coatings is currently not available. Whilst a method has been proposed by Wan et al. [48] to calculate the interfacial fracture energy between an elastic film and a stiff substrate by using shaft-loaded blister test, it is uncertain if it can be used for brittle ceramic coatings. The present authors tried to adopt this method for the present bioceramic coatings, and it was found that the application of this method was very limited due to the difficulty in sample preparation. It is doubtful if the method can be adapted for the thermal spray field.

4. Conclusions

The present study systematically investigated the different methods for determination of Young's modulus and fracture toughness of HVOF-sprayed HA and HA/titania coatings. Both the Young's modulus and fracture toughness are substantially dependent on coating microstructure and phase composition. Addition of titania (10 and 20 vol.%) was found to effectively improve the Young's modulus and fracture properties of HA coatings. Comparative results show that the three- and four-point bend tests are appropriate for measuring the overall Young's modulus of the coatings, while the indentation test is found to be strictly limited in its application due to the local-phase-dependent characteristics of the technique. Furthermore, the E values obtained using the indention test is influenced essentially by the surface roughness of the samples. Fracture toughness and strain energy release rate tests show a marked influence of coating structure. The cohesion between splats acts as the most important factor in determining the fracture properties of the thermal sprayed bioceramics coatings. It is found that the generally adopted bending test for the determination of strain energy pertaining to coating/substrate interface is less than adequate for the present bioceramics coatings. The main reason seems to lie in the poor cohesion of thermal-sprayed bioceramics relative to metallic coatings, which causes the bending-triggered cracks to propagate within the coating rather than the coating/substrate interface.

Acknowledgments

The authors thank Mr S.C. Chan for his helpful assistance in the measurement of Young's modulus using indentation process. The financial support by Nanyang Technological University of Singapore in the form of Research Scholarship for H. Li and research grant JT ARC 4/96 is also acknowledged.

References

[1] H. Kido, S. Saha, Proceedings of the Southern Biomedical Engineering Conference, IEEE, 1997, p. 272.
[2] B.C. Wang, T.M. Lee, E. Chang, C.Y. Yang, J. Biomed. Mater. Res. 27 (1993) 1315.
[3] T. Inadome, K. Hayashi, Y. Nakashima, H. Tsumura, Y. Sugioka, J. Biomed. Mater. Res. 29 (1995) 19.
[4] K. Hayashi, T. Inadome, T. Mashima, Y. Sugioka, J. Biomed. Mater. Res. 27 (1993) 557.
[5] K.A. Gross, B. Ben-Nissan, W.R. Walsh, E. Swarts, in: C. Coddet (Ed.), Thermal Spray: Meeting the Challenges of the 21st Century, Proceedings of the 15th International Thermal Spray Conference, Nice, France, 1998, p. 1133.
[6] L.-D. Piveteau, M.I. Girona, L. Schlapbach, P. Barbous, J.-P. Boilot, B. Gasser, J. Mater. Sic. Mater. Med. 10 (1999) 161.
[7] W. Bonfield, in: A. Pizzoferrato, P.G. Marchetti, A. Ravaglioli, A.J.C. Lee (Eds.), Biomaterials and Clinical Applications, Proceedings of the Sixth Conference for Biomaterials, Bologna, Italy, 1987, p. 13.
[8] Y.F. Chen, F. Erdogan, J. Mech. Phys. Solids 44 (1996) 771.
[9] H.G.P. Chung, M.V. Swain, T. Mori, Biomaterials 18 (1997) 1553.
[10] S.J. Howard, A.J. Phillips, T.W. Clyne, Composites 24 (1993) 103.
[11] I. Sevostianov, M. Kachanov, Acta. Mater. 48 (2000) 1361.
[12] S.H. Leigh, C.K. Lin, C.C. Berndt, J. Am. Ceram. Soc. 80 (1997) 2093.
[13] C.J. Li, A. Ohmori, R. McPherson, J. Mater. Sci. 32 (1997) 997.
[14] C.K. Lin, C.C. Berndt, J. Therm. Spray Technol. 3 (1994) 75.
[15] Y. Sugimura, M. Spector, Mater. Res. Soc. Symp. Proc. 550 (1999) 367.
[16] E. Harry, A. Rouzaud, M. Ignat, P. Juliet, Thin Solid Films 332 (1998) 195.
[17] A. Rouzaud, E. Barbier, J. Ernoult, E. Quesnel, Thin Solid Films 270 (1995) 270.
[18] N. Fawcett, Mater. Sci. Technol. 9 (1998) 2023.
[19] D. Rats, J. von Stebut, F. Augereau, Thin Solid Films 355 (1999) 347.
[20] D. Schneider, T. Schwarz, H.P. Buchkremer, D. Stoever, Thin Solid Films 224 (1993) 177.
[21] E. Champion, S. Gautier, D. Bernache-Assollant, J. Mater. Sci. Mater. Med. 7 (1996) 125.
[22] S. Gautier, E. Champion, D. Bernache-Assollant, J. Mater. Sci. Mater. Med. 10 (1999) 533.
[23] G.K. Beshish, C.W. Florey, F.J. Worzala, W.J. Lenling, J. Therm. Spray Technol. 2 (1993) 35.
[24] G. Qian, T. Nakamura, C.C. Berndt, S.H. Leigh, Acta Mater. 45 (1997) 1767.
[25] J.T. Krauser, P. Berthold, J. Dental Res. 70 (1991) 274.
[26] C.C. Chiu, J. Am. Ceram. Soc. 73 (1990) 1999.
[27] W.C. Oliver, G.M. Pharr, J. Mater. Res. 7 (1992) 1564.
[28] P.G. Charalambides, J. Lund, A.G. Evans, R.M. McMeeking, J. Appl. Mech. 56 (1989) 77.
[29] Y. Murakami (Ed.), Stress Intensity Factors Handbook, 3, Committee on Fracture Mechanics, The Society of Materials Science, Japan, 1992.
[30] A. Ravaglioli, A. Kraejewski, Bioceramics: Materials, Properties and Applications, Chapman and Hall, London, 1992.

[31] S.J. Scheider, Ceramics and Glasses, Engineering Materials Handbook, 4,, ASM International, The Materials Information Society, 1991.
[32] S.J. Howard, T.W. Clyne, Surf. Coat. Technol. 45 (1991) 333.
[33] A.G. Evans, M. Ruhle, B.J. Dalgleish, P.G. Charalambides, Mater. Sci. Eng. A 126 (1990) 53.
[34] H. Li, K.A. Khor, P. Cheang, Mater. Sci. Eng. A 293 (2000) 71.
[35] D.S. Metsger, M.R. Rieger, D.W. Foreman, J. Mater. Sci. Mater. Med. 10 (1999) 9.
[36] K.A. Gross, V. Gross, C.C. Berndt, J. Am. Ceram. Soc. 81 (1998) 106.
[37] L.J. Broutman, Fracture and Fatigue, Composite Materials, 5,, Academic Press, New York, 1974.
[38] H. Li, K.A. Khor, P. Cheang, Biomaterials 23 (2002) 85.
[39] P.J. Callus, C.C Berndt, Surf. Coat. Technol. 114 (1999) 114.
[40] Y. Yamada, R. Watanabe, Scrip. Mater. 34 (1996) 387.
[41] Y.C. Tsui, C. Doyle, T.W. Clyne, Biomateials 19 (1998) 2015.
[42] E. Lopez Cantera, B.G. Mellor, Mater. Lett. 37 (1998) 201.
[43] L.L. Shaw, B. Barber, E.H. Jordan, M. Gell, Scrip. Mater. 39 (1998) 1427.
[44] G.C. Sih, Mechanics of Fracture Initiation and Propagation, Kluwer Academic, USA, 1991.
[45] S. Ishihara, A.J. Mcevily, T. Goshima, K. Kanekasu, T. Nara, J. Mater. Sci. Mater. Med. 11 (2000) 661.
[46] D. Leguillon, Influence of micro-voids on toughness of interfaces, in: H.-P. Rossmanith (Ed.), Damage and Failure of Interface, Balkema, Rotterdam, 1997, p. 113.
[47] S.J. Howard, Y.C. Tsui, T.W. Clyne, Acta Metall. Mater. 42 (1994) 2823.
[48] K.T. Wan, Y. Mai, Int. J. Fracture 74 (1995) 181.